Electronic Supplementary Material (ESI) for RSC Advances.

SUPPORTING INFORMATION

Perylene Diimide Derivatives as Red and Deep Red-Emitters for Fully Solution Processable OLEDs

Erika Kozma*[1], Wojciech Mróz[1], Francesca Villafiorita-Monteleone[1], Francesco Galeotti[1], Anita Andicsová-Eckstein[2], Marinella Catellani[1], Chiara Botta[1]*

[1]*CNR-Istituto per lo Studio delle Macromolecole, Via Corti 12, 20133 Milano, Italy*

[2]*Polymer Institute, Slovak Academy of Sciences, Dúbravská cesta 9, SK-845 41 Bratislava, Slovak Republic*

*Corresponding authors. e-mail: erika.kozma@ismac.cnr.it, c.botta@ismac.cnr.it

TGA and DSC for PDI-1 and PDI-2

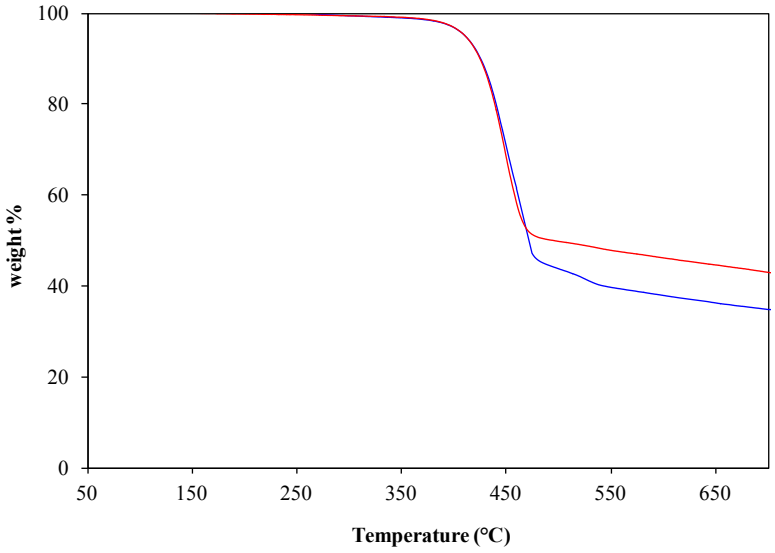

Figure ESI-1a. TGA curves of PDI-1 (—) and PDI-2(—) under inert atmosphere

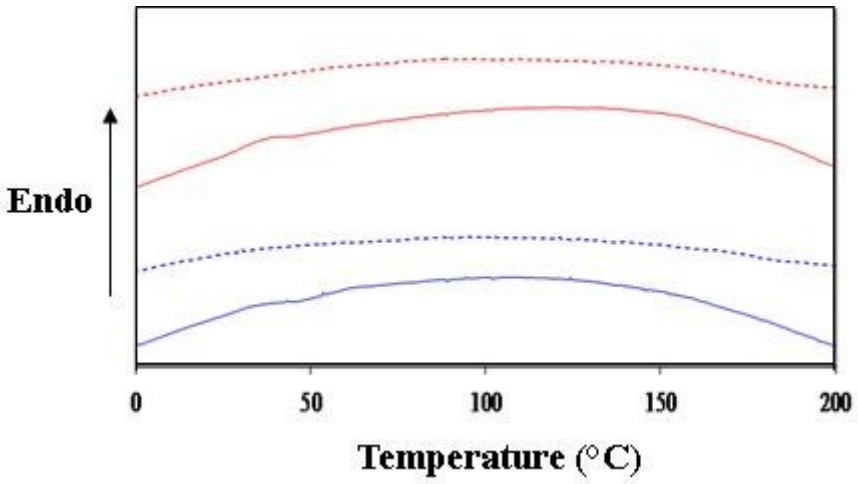

Figure ESI-1b. DSC scans of PDI-1 (—) and PDI-2 (—) from cooling (dashed line) and second heating (solid line) cycle.

Cyclic voltammetry of PDI-1 and PDI-2

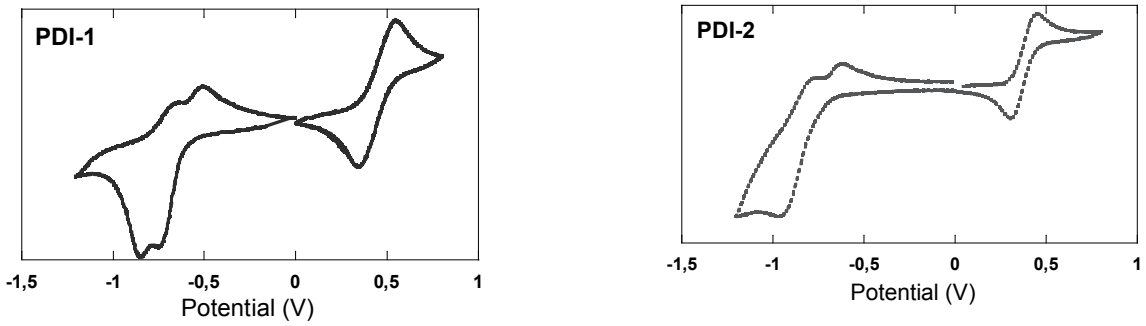

Figure ESI-2. Cyclic voltammograms of PDI-1 and PDI-2 thin films (internal standard ferrocene)

Table ESI-1. Electrochemical characteristics, experimental calculated HOMO-LUMO values and optical energy band gaps for PDI-1 and PDI-2

	E_{red}^{0}(V)	$E_{red}^{1/2}$(V)	E_{red}^{p}(V)	HOMO(eV)	LUMO(eV)	E_g^{opt}(eV)
PDI-1	-0.61	-0.67	-0.75	-5.79	-3.73	2.06
PDI-2	-0.59	-0.77	-0.80	-5.55	-3.63	1.92

Density functional theory calculations (DFT)

a **b**

Figure ESI-3a. Optimized structures of PDI-1 (a) and PDI-2 (b) obtained by DFT calculations at the B3LYP/6-31G** level.

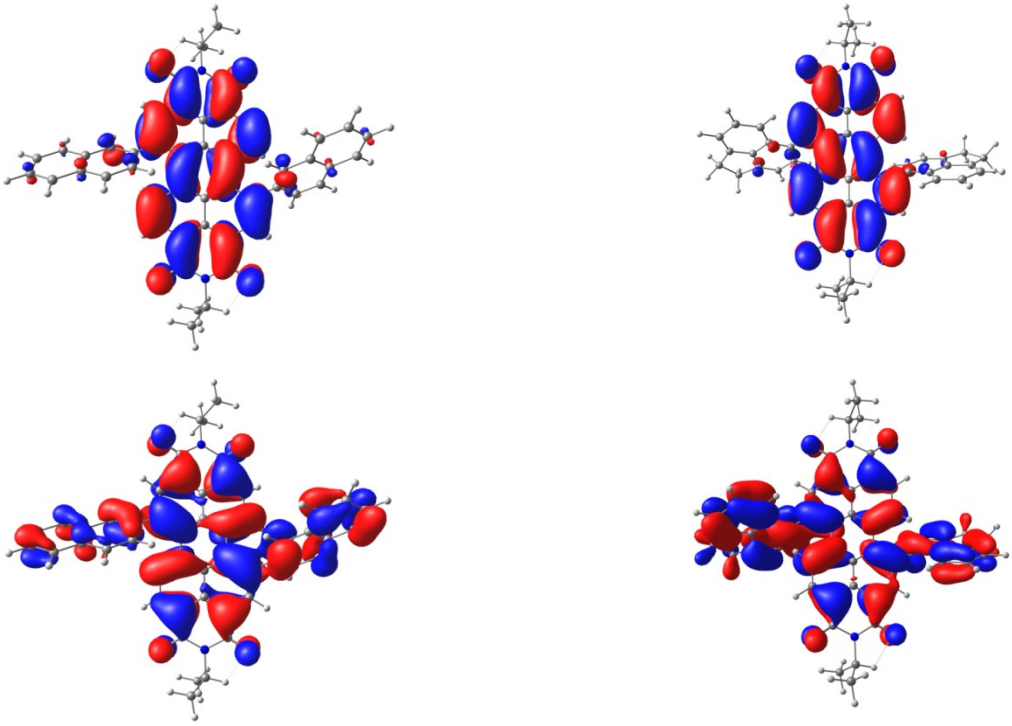

a **b**

Figure ESI-3b. Molecular orbital surfaces of the HOMO (bottom) and LUMO (top) of PDI-1 (a) and PDI-2(b) molecules obtained by DFT calculations at the B3LYP/6-31G** level.

Table ESI-2. Experimental and theoretically determinate (DFT) HOMO-LUMO energy values

	HOMO (eV)[a]	LUMO (eV)[a]	HOMO (eV)[b]	LUMO (eV)[b]
PDI-1	-5.79	-3.73	-5.64	-3.28
PDI-2	-5.55	-3.63	-5.47	-3.16

[a]determined from cyclic voltammetry reduction potentials ($E_{red}^{1/2}$) and optical band gap (E_g^{opt})
[b]determined with density functional theory (B3LYP/6-31G**)

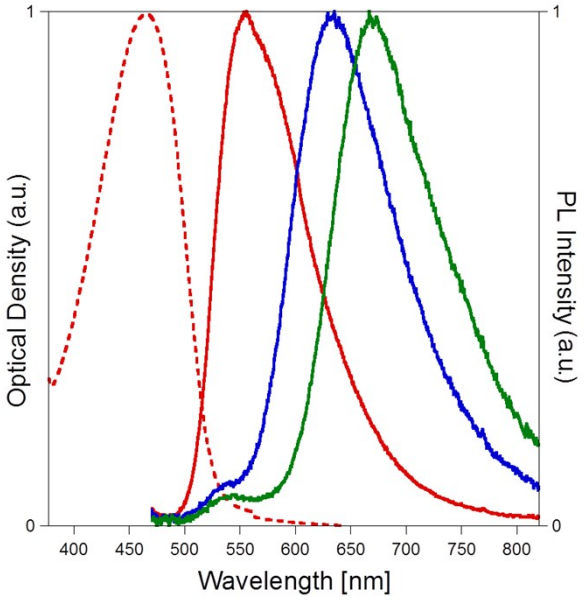

Figure ESI-4. Normalized spectra of F8BT cast film: absorption (dotted red line) and PL (red solid line); PL spectra F8BT/PDI blends (5% w/w): F8BT/**PDI-1** (blue solid line) and F8BT/**PDI-**2 (green solid line) (excitation at the absorption maximum of the polymer, 450 nm).

Table ESI-3. Optical properties of F8BT and of F8BT/**PDI-1** and F8BT/**PDI-2** blends (5% w/w) in the solid state

	Film		
Material	λ_{ab}[a] (nm)	λ_{em}[a] (nm)	QY[b] (%)
F8BT	463	550	45
F8BT-PDI-1	463	635	14
F8BT-PDI-2	463	668	21

[a]Spin coated films
[b]Cast films from toluene solution

AFM measurements

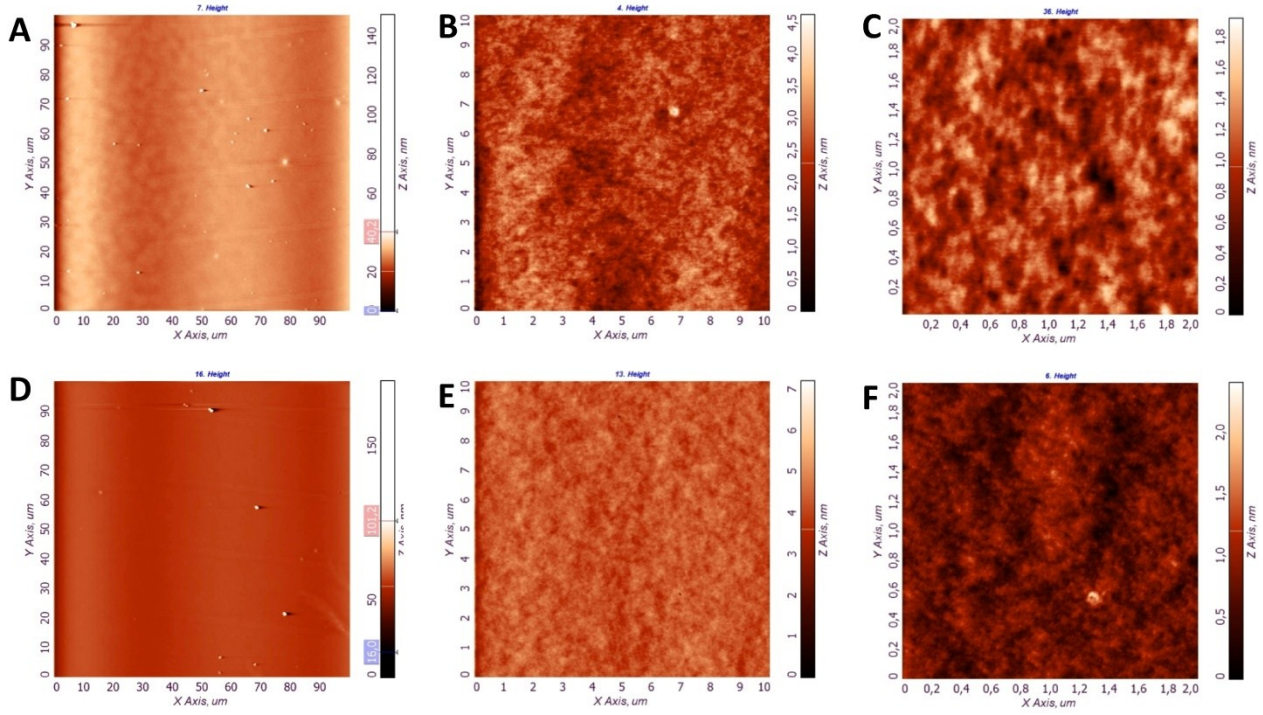

Figure ESI-5. AFM tapping-mode analysis of PDI-1 (A-C) and PDI-2 (D-F) single layer devices.

AFM analysis confirmed that both PDI-1 and PDI-2 have good film-forming properties. The large-area scans displayed in panels A and D of Fig. ESI-4 show that the homogeneity of the films on the OLEDs is interrupted only by the presence of a few small aggregated particles and no holes are present. The magnified views in panels B, C, E and F show that both films are characterized by similar low average roughness, resulting in root mean square values of 0.425 nm and 0.393 nm for PDI-1 and for PDI-2, respectively.

ESI-6. Structure of single layer and multilayer OLEDs

ITO(80nm)/PEDOT:PSS(45nm)/100% PDI-1(73nm)/Ba(7nm)/Al(100nm)
ITO(80nm)/PEDOT:PSS(45nm)/100% PDI-2(79nm)/Ba(7nm)/Al(100nm)

ITO(80nm)/PEDOT:PSS(45nm)/PVKc(55nm)/100% PDI-1(73nm)/PF-PEG(13nm)/Ba(7nm)/Al(100nm)
ITO(80nm)/PEDOT:PSS(45nm)/PVKc(56nm)/100% PDI-2(79nm)/PF-PEG(15nm)/Ba(7nm)/Al(100nm)

Figure ESI-7. Electroluminescence of simple and optimized OLEDs at different bias voltages